Journal of Marine Science and Application (2025) 24: 1064-1074
https://doi.org/10.1007/s11804-025-00637-0

RESEARCH ARTICLE

CFD-based Determination of Load Cell Capacity for Submarine HPMM Model Tests

Aliasghar Moghaddas[1], Hossein nourozi[2], Morteza Ebrahimi[3] and Alireza Naderi[4]

Received: 17 February 2024 / Accepted: 17 November 2024

Abstract

Captive model tests are one of the most common methods to calculate the maneuvering hydrodynamic coefficients and characteristics of surface and underwater vehicles. Considerable attention must be paid to selecting and designing the most suitable laboratory equipment for towing tanks. A computational fluid dynamics (CFD) -based method is implemented to determine the loads acting on the towing facility of the submarine model. A reversed topology is also used to ensure the appropriateness of the load cells in the developed method. In this study, the numerical simulations were evaluated using the experimental results of the SUBOFF benchmark submarine model of the Defence Advanced Research Projects Agency. The maximum and minimum loads acting on the 2.5-meter submarine model were measured by determining the body's lightest and heaviest maneuvering test scenarios. In addition to having sufficient endurance against high loads, the precision in measuring the light load was also investigated. The horizontal planar motion mechanism (HPMM) facilities in the National Iranian Marine Laboratory were developed by locating the load cells inside the submarine model. The results were presented as a case study. A numerical-based method was developed to obtain the appropriate load measurement facilities. Load cells of HPMM test basins can be selected by following the two-way procedure presented in this study.

Keywords Captive model tests; Hydrodynamic coefficients; Submarine; Computational fluid dynamics; Horizontal planar motion mechanism; Load cell capacity

1 Introduction

With the development of the marine industry, high-precision instruments are fundamental in designing and analyzing marine vehicles in marine laboratories. Maneuverability is a major factor affecting the performance of marine underwater vehicles. Maneuver simulations based on mathematical models are widely used to predict motion parameters. A key stage in applying a mathematical model is the determination of the hydrodynamic coefficients. Captive model tests are well-known methods for calculating the hydrodynamic coefficients of ships and submarines. Owing to the port-starboard symmetry of the conventional marine vehicles, dependence on some movements is reduced, and the body's movement can be studied separately in two horizontal and vertical planes. Captive model tests are currently the most reliable method to obtain the maneuvering hydrodynamic coefficients of marine vehicles. In these tests, the body movement is restrained to the carriage mechanism by one or more arms. Owing to the high sensitivity of forces in light tests, the laboratory should be equipped with high-precision equipment that can cover the high forces in heavy-duty tests. The correct selection of load cells and the design of the arm structure require the prediction of the forces with the highest possible accuracy.

Many researchers have conducted numerical and experimental studies on submarine maneuvers. Owing to the high costs of the model tests, numerical methods are considered an appropriate method for estimating the hydrodynamic derivatives and loads acting on the model in the initial state of design. Computational fluid dynamics (CFD) has provided a wide environment for various hydrodynamic

Article Highlights

- The maximum and minimum loads acting on the 2.5-meter submarine model were measured by determining the body's lightest and heaviest maneuvering test scenarios.
- The horizontal planar motion mechanism (HPMM) facilities in the National Iranian Marine Laboratory were developed by locating the load cells inside the submarine model.
- Load cells of HPMM test basins can be selected by following the two-way procedure presented in this study.

✉ Aliasghar Moghaddas
moghaddas@aut.ac.ir

[1] Marine Research Center, Imam Hossein Comprehensive University, Tehran 11369, Iran

[2] Mechanical Engineering Department, Malek Ashtar University of Technology, Tehran 11369, Iran

[3] National Iranian Marine Laboratory (NIMALA), Tehran 11369, Iran

[4] Marine Engineering Department, Amirkabir University of Technology, Tehran 11369, Iran

analyses and new methods, such as dynamic tests conducted (Ziabari and Mousavizadegan, 2024). Therefore, the current study prefers it over other numerical methods. To date, less attention has been paid to the design process of test mechanisms in towing tanks. The hydrodynamic coefficients of the SUBOFF body was investigated numerically using the finite volume method to solve Reynolds Average Navier–Stokes (RANS) equations (Pan et al., 2012). numerically simulated the captive model tests in horizontal and vertical planes to investigate the maneuvering derivatives of a submarine with cross-shaped fins. Except for surge motion, all the body movements were defined in an internal region near the body surface to precisely simulate the planar motions (Cho et al., 2020). The effects of side walls was investigated in circulating flow channels and strut arms on the hydrodynamic coefficients of an autonomous submarine. Dimensionless width parameters were used to reduce the dependence between channel width and hydrodynamic coefficients of the model. The results demonstrated that the hydrodynamic coefficients increased with the tank width (Huang et al., 2020). The velocity and amplitude of the body motion in planar motion mechanism (PMM) tests for an ellipse numerically investigated (Ardeshiri et al., 2020). Furthermore, several numerical and experimental approaches were adopted to generate a captive model for surface vessels in 3-DOF (Yoon et al., 2015a; Yoon et al., 2015b; Zhu et al., 2022).

PMM tests are classified into two main categories, namely, horizontal planar motion mechanism (HPMM) and vertical plane motion mechanisms (VPMM). Considering the facilities of the National Iranian Marine Laboratory (NIMALA), this study investigated the horizontal planar motion mechanism. The HPMM mechanism must be able to move the model in three degrees of freedom and measure the moment and forces acting on the model's hull. In the HPMM of David Taylor's laboratory, two upper arms were tied to the model to provide translational and rotational motions (Roddy, 1990). Another study use model binding with two arms and two double-component load cells (Kim, 2023). Also a research, used a strut stretched to the model tail to carry the model, in which the moment and forces were measured by a three-component load cell (Park et al., 2017).

The equipment for HPMM tests should be selected based on laboratory specifications, such as tank dimensions and towing speed. Given that heavy and light loads are measured by load cells during the HPMM tests in towing tanks, improper estimation of the force values may cause untended consequences affecting the accuracy of the test results. Selecting too low-capacity load cells will cause damage to the facilities. However, if the selected load cells are too high-capacity, the accuracy of the load measurement in the light tests may decrease.

This topology offers a proper estimation of the hydrodynamic loads acting on the model's body according to the specified test scenarios. The whole test process is simulated in the CFD numerical environment to consider the specifications of the laboratory facilities and the probable bodies to be tested. Some of the benefits of using CFD in this work include its precision in the direct calculation of the loads and its consideration of the special geometry and various test conditions of the laboratory. Therefore, it is preferred over common empirical estimation methods.

Owing to the lack of a specific guideline for the HPMM load cell selection in marine laboratories, the instructions presented in this paper can be followed for similar works.

In this study, the HPMM mechanism is selected by considering the predicted loads obtained from the CFD simulations. The load cells are controlled in terms of force tolerance and sufficient accuracy using the criteria calculated by numerical analysis and those set by the manufacturer of the load cells. A mechanism in which the load cells are located inside the body is designed to remove the hydrodynamic forces of the carriage arms. Analysis is performed to predict whether the force on the load cells originates only from the hydrodynamic forces acting on the body.

2 Governing equations

2.1 Equations of motion

In general, the motion equations of a marine vehicle can be expressed in six degrees of freedom. Two coordinate systems are defined for the vessel, namely, the earth-fixed coordinate system and the body-fixed coordinate system that is stuck to the body and always moves with it. These two coordinate systems are shown in Figure 1. The equations of motion in the body-fixed coordinate system are as follows (Fossen, 1994):

$$\boldsymbol{M}_{\mathrm{RB}}\dot{\boldsymbol{v}} + \boldsymbol{C}_{\mathrm{RB}}\boldsymbol{v} = \boldsymbol{\tau}_{\mathrm{RB}} \tag{1}$$

where $\boldsymbol{M}_{\mathrm{RB}}$ is the inertial matrix, and $\boldsymbol{C}_{\mathrm{RB}}$ is the Coriolis matrix of the body. The values of these two matrices depend on the body's weight distribution. $\boldsymbol{v} = \{u, v, w, p, q, r\}^{\mathrm{T}}$ is the velocity vector, in which the first three terms are translational velocities in the direction of the x, y, and z axes, and

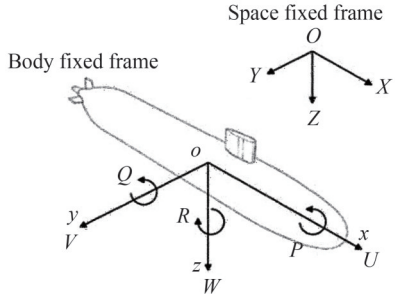

Figure 1 Earth-fixed and body-fixed coordinate systems

the second three terms are the respective rotational velocities. $\dot{\boldsymbol{v}} = \{\dot{u}, \dot{v}, \dot{w}, \dot{p}, \dot{q}, \dot{r}\}^{\mathrm{T}}$ is the vector of translational and rotational accelerations. $\boldsymbol{\tau}_{\mathrm{RB}}$ is the external force and moment matrix including hydrostatic and hydrodynamic forces.

Under the following assumptions, the hydrodynamic forces and moments of the body due to the movement speed and acceleration under the water can be separated from the other external forces.

• The submarine moves deep enough that the free surface does not affect its forces and moments.

• Motion is only provided by the propulsion system.

• Control surfaces are in equilibrium condition and do not change the direction of motion.

Under the above assumptions, the matrix of external forces and moments is equal to that of force and hydrodynamic moments as follows:

$$\boldsymbol{\tau}_{\mathrm{RB}} = \boldsymbol{\tau}_h = \{X, Y, Z, K, M, N\}^{\mathrm{T}} \tag{2}$$

Therefore, X, Y, and Z are the external forces acting on the body in the x (surge), y (sway), and z (heave) directions, respectively; K, M, and N are the external moments in ϕ (roll), θ (pitch), and ψ (yaw), respectively. expressing these forces and moments using velocities and hydrodynamic coefficients is as the following forms (Getler and Hagen, 1967):

$$\begin{aligned} X = {} & \frac{1}{2}\rho l^4\left(X'_{qq}q^2 + X'_{rr}r^2 + X'_{rp}rp\right) + \\ & \frac{1}{2}\rho l^3\left(X'_{\dot{u}}\dot{u} + X'_{vr}vr + X'_{wq}wq\right) + \\ & \frac{1}{2}\rho l^2\left(X'_{uu}u^2 + X'_{vv}r^2 + X'_{ww}w^2\right) \end{aligned} \tag{3}$$

$$\begin{aligned} Y = {} & \frac{1}{2}\rho l^4\left(Y'_{\dot{r}}\dot{r} + Y'_{\dot{p}}\dot{p} + Y'_{p|p|}p|p| + Y'_{qr}qr\right) + \\ & \frac{1}{2}\rho l^3\left(Y'_{\dot{v}}\dot{v} + Y'_{vq}vq + Y'_{wp}wp + Y'_{wr}wr + Y'_{r}ur + \right. \\ & \left. Y'_{p}up + Y'_{v|r|}\frac{v}{v|r|}\left|\left(v^2 + w^2\right)^{\frac{1}{2}}\right||r|\right) + \\ & \frac{1}{2}\rho l^2\left(Y'_{*}u^2 + Y'_{v}uv + Y'_{v|v|}v\left|\left(v^2 + w^2\right)^{\frac{1}{2}}\right| + Y'_{vw}vw\right) \end{aligned} \tag{4}$$

$$\begin{aligned} Z = {} & \frac{1}{2}\rho l^4\left(Z'_{\dot{q}}\dot{q} + Z'_{pp}p^2 + Z'_{rr}r^2 + Z'_{rp}rp\right) + \frac{1}{2}\rho l^3\left(Z'_{\dot{w}}\dot{w} + \right. \\ & \left. Z'_{vr}vr + Z'_{vp}vp + Z'_{q}uq + Z'_{w|q|}\frac{w}{|w|}\left|\left(v^2 + w^2\right)^{\frac{1}{2}}\right||q|\right) + \\ & \frac{1}{2}\rho l^2\left(Z'_{*}u^2 + Z'_{v}uv + Z'_{w}uw + Z'_{w|w|}w\left|\left(v^2 + w^2\right)^{\frac{1}{2}}\right| + Z'_{vv}v^2\right) \end{aligned} \tag{5}$$

$$\begin{aligned} K = {} & \frac{1}{2}\rho l^5\left(K'_{\dot{p}}\dot{p} + K'_{\dot{r}}\dot{r} + K'_{qr}qr + K'_{pq}pq + K'_{p|p|}p|p|\right) + \\ & \frac{1}{2}\rho l^4\left(K'_{\dot{v}}\dot{v} + K'_{vq}vq + K'_{wp}wp + K'_{wr}wr\right) + \\ & \frac{1}{2}\rho l^3\left(K'_{*}u^2 + K'_{v}uv + K'_{v|v|}\left|v\left(v^2 + w^2\right)^{\frac{1}{2}}\right| + K'_{vw}vw\right) \end{aligned} \tag{6}$$

$$\begin{aligned} M = {} & \frac{1}{2}\rho l^5\left(M'_{\dot{q}}\dot{q} + M'_{pp}p^2 + M'_{rr}r^2 + M'_{rp}rp + \right. \\ & \left. M'_{p|p|}p|p|\right) + \frac{1}{2}\rho l^4\left(M'_{\dot{w}}\dot{w} + M'_{vr}vr + M'_{vp}vp + \right. \\ & \left. M'_{q}uq + M'_{q|w|}\left|\left(v^2 + w^2\right)^{\frac{1}{2}}\right|q\right) + \\ & \frac{1}{2}\rho l^3\left(M'_{*}u^2 + M'_{w}uw + M'_{w|w|}w\left|\left(v^2 + w^2\right)^{\frac{1}{2}}\right| + \right. \\ & \left. M'_{|w|}u|w| + M'_{ww}\left|w\left(v^2 + w^2\right)^{\frac{1}{2}}\right| + M'_{vv}v^2\right) \end{aligned} \tag{7}$$

$$\begin{aligned} N = {} & \frac{1}{2}\rho l^5\left(N'_{\dot{r}}\dot{r} + N'_{\dot{p}}\dot{p} + N'_{pq}pq + N'_{qr}qr + N'_{r|r|}r|r|\right) + \\ & \frac{1}{2}\rho l^4\left(N'_{\dot{v}}\dot{v} + N'_{wr}wr + N'_{wp}wp + N'_{vq}vq + N'_{p}up + \right. \\ & \left. N'_{r}ur + N'_{v|r|}\left|\left(v^2 + w^2\right)^{\frac{1}{2}}\right|r\right) + \frac{1}{2}\rho l^3\left(N'_{*}u^2 + \right. \\ & \left. N'_{v}uv + N'_{v|v|}v\left|\left(v^2 + w^2\right)^{\frac{1}{2}}\right| + N'_{vw}vw\right) \end{aligned} \tag{8}$$

where m expresses the mass, and I_x, I_y, and I_z are the inertia moment of each axis. The translational velocities in the directions of surge, sway, and heave are expressed by u, v, and w, respectively, and the angular velocities around these axes are expressed by p, q, and r, respectively. Translational and rotational accelerations are displayed in the formulas with the derivative sign on the velocity components. $Y'_{\dot{r}}$, $X'_{\dot{u}}$, $Z'_{\dot{q}}$, ⋯ are the added mass hydrodynamic coefficients, and X'_{rr}, $M'_{p|p|}$, N'_{p}, ⋯ are the damping hydrodynamic coefficients presented in a non-dimensional form.

2.2 Fluid dynamic equations

The governing equations are the conservation of mass and Navier–Stokes equations in three dimensions, which can be expressed as RANS equations by assuming viscosity and incompressibility. RANS equations are used to simulate the fluid flow around a submarine body in CFD for calculating force and torque. The variables of velocity and pressure are divided into average and fluctuating terms. RANS equations are expressed as follows (Ferizer and Peric, 2002):

$$\frac{\partial\left(\rho\overline{u_i}\right)}{\partial t}+\frac{\partial}{\partial x_j}\left(\rho\overline{u_i}\,\overline{u_j}+\rho\overline{u_i'u_j'}\right)= \frac{\partial\bar{p}}{\partial x_i}+\rho g_i+\mu\frac{\partial}{\partial x_j}\left(\frac{\partial\overline{u_j}}{\partial x_i}+\frac{\partial\overline{u_i}}{\partial x_j}\right) \quad (9)$$

$$\frac{\partial\left(\rho\bar{u}_i\right)}{\partial x_i}=0 \quad (10)$$

where μ, ρ, and $\bar{p}$ represent viscosity, density, and timed-average pressure, respectively. In Equation (10), $\tau_{ij}=\overline{u_i'u_j'}$ is the Reynolds stress term that includes the effects of turbulence on the average stress. In this study, the two equations model k–ε is chosen to solve the Reynolds stress equation (Shih et al., 1994).

3 Verification

The captive model test is applied to calculate the hydrodynamic coefficients of damping and added mass on the SUBOFF bare hull body with 4.35 m length and 0.508 m diameter (Groves et al., 1989). The simulations are performed in static and dynamic conditions. For checking the precision of the numerical solution, the static drift test is selected among the static tests and the pure yaw test is selected among the dynamic tests.

3.1 Computational domain and mesh study

For the numerical solution, creating a computational domain around the body and defining its boundary conditions are necessary. Given that the selected scenarios for verification are based on the tests conducted in David Taylor's laboratory, the width of the computing domain is also adopted from the same tests. The computational domain and boundary conditions of the numerical solution are specified in Figure 2. The same computational domain is specified for the static and dynamic test simulations.

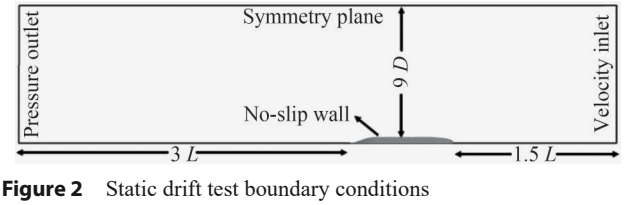

Figure 2 Static drift test boundary conditions

Simulations in CFD are highly dependent on the generated mesh. This study uses the trimmer mesh produced by Star CCM+, as shown in Figure 3. In the static drift test simulation, which is in steady-state, the domain mesh is fixed, and the forward movement of the model is simulated by the inlet flow. However, in the pure yaw test, a dynamic mesh in which the whole computational domain moves within the body movements is used due to the submarine motion. In the dynamic mesh simulation, the generated mesh is modified during the simulation to accommodate the geometrical changes, such as translating and rotating boundaries. Compared with selecting a fixed domain and moving the body surface, this procedure dramatically reduces the calculation time.

Table 1 Summary of numerical setup

Setting	Description
Time	Implicit unsteady
Time step (for pure yaw) (s)	0.005
Iteration per time step	5
Flow	Segregated flow
Equation of state	Constant density
Turbulence model	Realizable K-Epsilon
Pressure link	SIMPLE

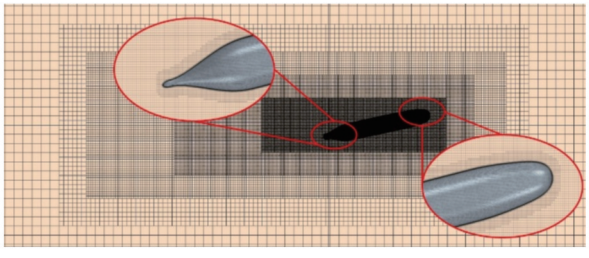

Figure 3 DARPA SUBOFF maneuver simulation grid

Verification must be performed to ensure that appropriate results are calculated from the numerical simulations. In this work, a mesh convergence study is applied to verify the numerical simulations (ITTC, 2017). Three different meshes with a ratio of $\sqrt{2}$ are considered. The force in the longitudinal and transverse directions and the yaw moment at the drift angle of 12° are calculated in the three mentioned states. In Figure 4, the results of the numerical simulations are shown in different meshing modes for the calculated forces and moments. Starting from the second case, increasing the number of grids does not significantly affect the forces and moments, and the solution is independent of the number of grids.

In this study, the solver results and the quality of the grid are evaluated by the grid convergence index (GCI), which estimates the discretization error. GCI is defined as follows (Celik et al., 2008):

$$\mathrm{GCI}_{i,i+1}=\frac{F_s\left|e_{i,i+1}\right|}{r_{i,i+1}^{p}-1} \quad (11)$$

where F_s is the safety factor equal to 1.25. For checking the convergence of more than two states, $e_{i,i+1}$ shows the relative error between two states, and r is the correction

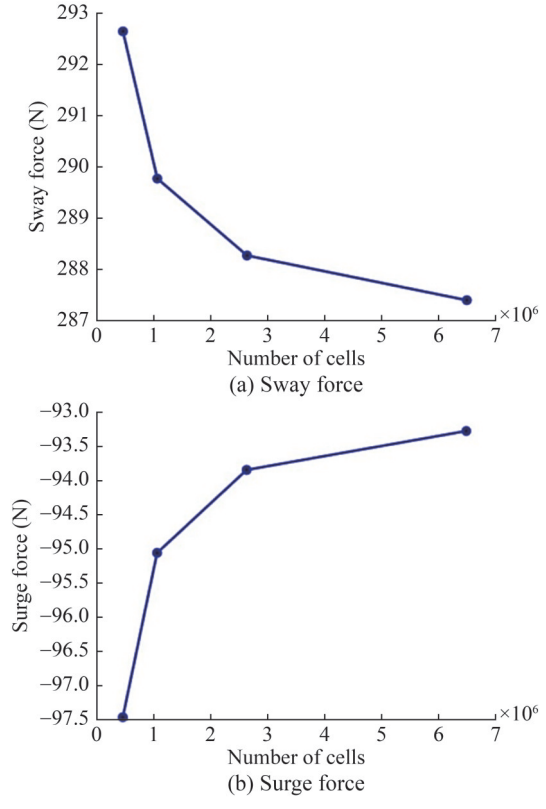

Figure 4 Mesh independency for surge and sway force

factor. The convergence ratio and discretization order are indicated by R and P, respectively.

The results for the grid formed for the numerical solution of the static drift test at the drift angle of 12° are shown in Table 2. According to the values of GCI and R, the convergence criteria for medium and fine meshing are acceptable, and the numerical solution is independent of the number of meshes. A grid system with a number of 2.6 million cells is used for the continuation of the simulations of the SUBOFF body maneuver. The steady run used for the static drift test has taken 4.15, 8.89, and 29.74 h at the 1 500th iteration for the course, medium, and fine grids, respectively.

Owing to the boundary conditions of the no-slip wall for the floating body, the fluid flow near the body is strongly affected and causes large changes in the fluid velocity. Therefore, the wall function and prismatic layered grid are used to accurately simulate the flow near the wall. The value of the prismatic layered network components is determined based on y^+ according to Equation (12).

$$y^+ = \frac{y \cdot u^*}{v} \tag{12}$$

where y is the distance of the first node to the wall, v is the dynamic viscosity, and u^* is the characteristic velocity of the turbulent flow. According to ITTC recommendation, the value of y^+ in turbulent flows should be between 30 and 300 (ITTC, 2014). The value of y^+ at the drift angle of 12° for the SUBOFF bare hull is shown in Figure 5. Most parts of the body surfaces are in the log layer zone with y^+ value more than 30. The all-y^+ treatment is applied to the numerical solver in STAR CCM+ to eliminate the concern of the parts with y^+ values in the buffer region (Siemens, 2021). This treatment is suitable for a wide range of boundary layer mesh densities, including the instance when the wall-cell centroid falls in the buffer region of the boundary layer.

Table 2 Values of mesh independency analysis parameters based on the roache method

Parameter	Sway force	Yaw moment	Surge force
N_1 (Coarse)	1 060 150	-	-
N_2 (Medium)	2 633 531	-	-
N_2 (Fine)	6 491 859	-	-
ϕ_1	289.773	−1 053.30	−95.056
ϕ_2	288.27	−1 054.784	−93.84
ϕ_3	287.396	−1 055.51	−93.27
P	0.588 76	0.770 28	0.826 44
R	0.581 5	0.493 2	0.468 8
GCI (coarse-medium)	0.919 65%	0.172 71%	1.444 7%
GCI (medium-fine)	0.542 32%	0.086 13%	0.689 59%

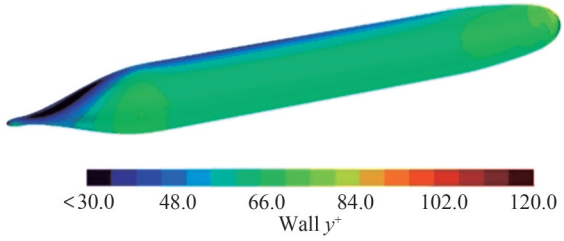

Figure 5 y^+ distribution on SUBOFF body in static drift test

3.2 Calculation of hydrodynamic coefficients

3.2.1 Static drift

The static drift tests and pure yaw of SUBOFF in the simulations are according to the tests conducted in David Taylor's laboratory. In its static drift test, the model is pulled forward by the carriage at a speed of 6.5 kn, and the submarine body is connected to the carriage's arms from −18 to +18. In this study, static drift simulations are performed for the drift angles of −16° to +16° for the bare hull of the SUBOFF model. The nondimension form of force and torque are as follows (Feldman, 1979):

$$N' = \frac{N}{0.5\rho L^3 U^2} \tag{13}$$

$$Y' = \frac{Y}{0.5\rho L^2 U^2} \tag{14}$$

By knowing the drift angle in each simulation and the relation of the sway velocity according to the drift angle, the sway velocity can be calculated using Equation (15).

$$v = U \sin\beta \tag{15}$$

The numerical simulation results are shown as black dots in Figure 6. The most optimal curve from the numerical results must be crossed to obtain the hydrodynamic coefficients according to the following equation:

$$y = ax + bx^3 \tag{16}$$

where y is the dimensionless sway force or dimensionless yaw moment, a is the linear hydrodynamic coefficient (Y'_v or N'_v), and b is the nonlinear hydrodynamic coefficient (Y'_{vvv} or N'_{vvv}). The graphs are fitted using the curve fitting tool in MATLAB. The hydrodynamic coefficients obtained from the analysis of computational fluid dynamics results are compared with the experimental results in Table 3.

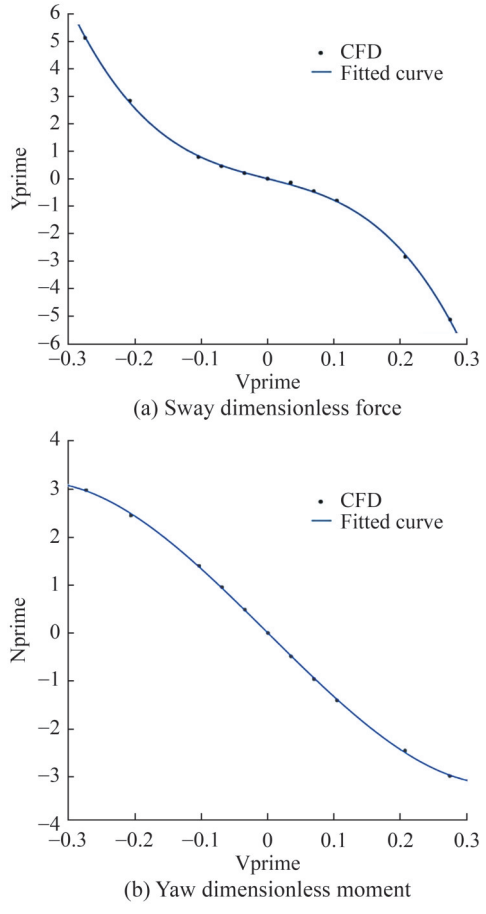

Figure 6 Numerical simulation results and fitted charts in static drift test

3.2.2 Pure yaw

In obtaining the hydrodynamic coefficients related to yaw movement, the submarine transverse motions must be limited and its head angle must always be tangent to the path. The pure yaw motion is applied to the model and computational domain using the following relations:

$$\psi = -\psi_0 \cos(2\pi\omega t) \tag{17}$$

$$r = \psi_0(2\pi\omega)\sin(2\pi\omega t) \tag{18}$$

$$\dot{r} = \psi_0(2\pi\omega)^2 \sin(2\pi\omega t) \tag{19}$$

where ψ_0 is the maximum heading angle, ψ is the yaw angle, and ω is the frequency of yaw motion. The pure yaw reference test is performed at a fixed motion frequency of 0.353 Hz and forward speed of 4.5, 5, 6, and 6.5 kn. In this study, only the forward speed of 6.5 kn is investigated. One of the methods for calculating hydrodynamic coefficients from the force and torque output diagrams of dynamic maneuver tests is to apply the linear regression method. The calculation results at each time step are recorded in CFD. By knowing the test scenario, the force, speed, and acceleration matrices can be written as follows (Foroushani and Sabzpooshani, 2021):

$$\underbrace{\begin{bmatrix}\theta_1\\ \theta_2\\ \vdots\\ \theta_n\end{bmatrix}}_{\boldsymbol{\theta}} = \underbrace{\begin{bmatrix}u_1 & \cdots & r_1 & \dot{u}_1 & \cdots & \dot{r}_1\\ u_2 & \cdots & r_2 & \dot{u}_2 & \cdots & \dot{r}_2\\ \vdots & & \vdots & \vdots & & \vdots\\ u_n & \cdots & r_n & \dot{u}_n & \cdots & \dot{r}_n\end{bmatrix}}_{\boldsymbol{\varphi}} \underbrace{\begin{bmatrix}\psi_n\\ \vdots\\ \psi_r\\ \psi_{\dot{u}}\\ \vdots\\ \psi_{\dot{r}}\end{bmatrix}}_{\boldsymbol{\psi}} \tag{20}$$

where each row of the $\boldsymbol{\theta}$ matrix shows the amount of force or torque in one time step of the solution. n is the number of data points extracted from numerical simulation. The more data points, the more accurate the curve fitting and the extraction of hydrodynamic coefficients. Increasing the number of data points may increase the calculation time without significantly affecting the results. The matrix $\boldsymbol{\varphi}$ expresses the speed and accelerations at each time step, and $\boldsymbol{\psi}$ is the matrix of hydrodynamic coefficients. The matrix of hydrodynamic coefficients can be calculated as follows using the inverse and determinant of the velocity and acceleration matrix:

Table 3 Hydrodynamic coefficients obtained from static drift tests using numerical and experimental approaches

Coefficient	CFD	EFD	Error (%)
Y'_v	−0.006 128	−0.005 948	3.03
N'_v	−0.013 61	−0.012 795	6.37
Y'_{vvv}	−0.165 6	-	-
N'_{vvv}	0.037 73	-	-

$$\boldsymbol{\psi} = \left(\boldsymbol{\varphi}^{\mathrm{T}}\boldsymbol{\varphi}\right)^{-1}\boldsymbol{\varphi}^{\mathrm{T}}\boldsymbol{\theta} \tag{21}$$

The optimal diagram fitted to the force and moment points obtained from the numerical simulation in the pure yaw test is shown in Figure 7. Hydrodynamic coefficients related to yaw motion are also described in Table 4.

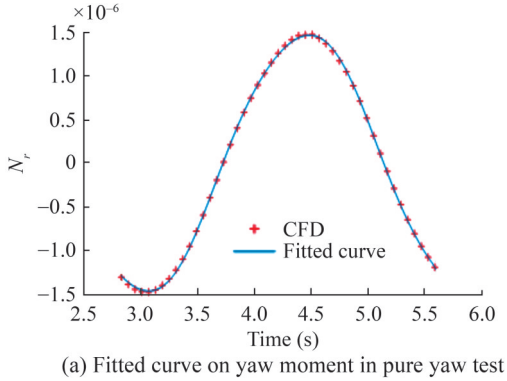

(a) Fitted curve on yaw moment in pure yaw test

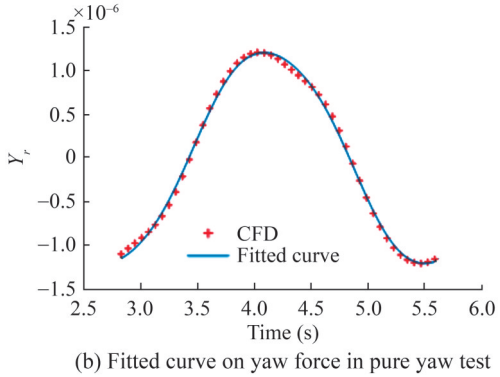

(b) Fitted curve on yaw force in pure yaw test

Figure 7 Diagram of the fitted curves and the points obtained from the pure yaw numerical simulation

Table 4 Hydrodynamic coefficients obtained from pure yaw test in numerical simulation and laboratory experiment

Coefficient	CFD	EFD	Error (%)
Y_r'	0.001 03	0.001 811	43.13
N_r'	−0.001 13	−0.001 597	29.24
$Y_{\dot{r}}'$	0.000 258	0.000 060	330
$N_{\dot{r}}'$	−0.000 76	−0.000 676	12.43

4 Determining the capacity and type of load cells

Test scenario for calculating maximum forces. The submarine model for testing in the NIMALA must have dimensions suitable for the tank dimensions. The goal of this study is to select the most appropriate load cells suitable for this facility. The first step of load cell selection is modeling a submarine model with the largest allowable dimensions from a hydrodynamic point of view. The main specifications of the NIMALA towing tank are given in Table 5. ITTC recommendations (ITTC, 2021) stipulate the framework of the HPMM tests, including the model dimensions and test scenario details.

Table 5 Characteristics of the National Iranian Persian Gulf Towing Tank

Parameter	Value
Length (m)	400
Width (m)	6
Depth (m)	4
Density of water (kg/m^3)	1 002
Kinematic viscosity of water	9.75×10^{-7}
Maximum velocity of the carrier (m/s)	18

The free surface effect is one of the effects that should be avoided in the test. With the distance set as five times the diameter from the top of the submarine model from the water surface, the distance of the top of the submarine model from the surface should be 1.9 m. This value is the lowest allowed depth and makes the floor effects negligible. The geometric characteristics of the submarine model determined for the analysis are described in Table 6.

Table 6 Geometric characteristics of the tested submarine body

Quantity	Value
Length (m)	2.5
Diameter (m)	0.254
Number of control surfaces	4
LCG (m)	1.428 68
Mass (kg)	100.62
I_{zz} (kg·m^2)	34.702 4

The last limitation of the laboratory environment is the speed limit. According to ITTC instructions, the maximum speed should be less than the $\sqrt{gh}/2$ to remove the effects of the wall and the floor. Therefore, with the depth of immersion being known, the selected speed should be less than 2.27 m/s. In this work, the forward speed selected for the tests is 2.25 m/s. According to the ITTC instructions, the ratio of the length of the model to the width of the tank should be less than 0.45 to eliminate the effect of the wall in harmonic tests. Considering the 6-meter width of the tank, the 2.5-meter model is selected.

The maximum forces that may be applied to the selected load cells during various tests should be predicted using numerical simulation. The heaviest scenario for the submarine maneuver test in the NIMALA is the combined yaw and drift test at the frequency of 0.35 Hz and the maximum drift angle of 30°. This test scenario is arranged according to some the criteria to determine the exact capacity of load cells using numerical analysis in CFD (Vantorre, 2000). The debatable point at this stage is determining the selec-

tion process of load cells. Two two-component load cells are selected according to the flowchart in Figure 8.

4.1 Numerical results

4.1.1 Hydrodynamic forces acting on the body

Given that all the linear and nonlinear forces and moments are present in the acting loads to the load cells, the estimation method must consist of nonlinear, cross-coupling, and added mass terms. Several empirical and analytical approaches can be employed for calculating the hydrodynamic coefficients of the submarine model, and each of them can estimate a limited set of hydrodynamic coefficients. However, some of the cross-coupling terms will be unestimated, even by combining different methods (Holmes and Papoulias, 1995; Kepler, 2018; Humphreys and Watkinson, 1978). Furthermore, the full appendage model submarine model of this study is different from other benchmark models. Therefore, these methods are not sufficiently precise to calculate the forces and moments acting on the body in the drift–yaw test. In the present study, the loads acting on each load cell are directly calculated by simulating the test scenarios in CFD.

The results of the numerical analysis related to the static drift test, pure sway, pure yaw, and combined drift–yaw tests are used to determine the capacity of the load cells. The graphs in Figure 9 show the results of transverse forces calculated in computational fluid dynamics in the heaviest test scenario. Simulations are stopped when the third cycle of the oscillatory motion is finished at the physical time of 8.57 s. The first two cycles are not taken into account due to a lack of convergence in numerical solving. The total CPU time spent for the drift–yaw simulation equals 78 h, which was done by a 9th generation core I7 CPU with 32 GB RAM.

It should be noted that the minimum load that can be measured by load cells is usually 0.2% of its maximum capacity. Therefore, according to the minimum force acting on the body and considering this percentage, the maximum capacity of the load cell can be calculated. The forces acting on the model in different test scenarios are described in Table 7. As expected, the maximum forces appeared in the combined drift–yaw test, and the minimum forces were recorded in the static drift test.

4.1.2 Determining the force on each load cell

The load measured by each of the load cells during the test is affected by the two components of force and moment, which are extracted from the numerical simulations. In the predicted mechanism for testing the submarine model, each of the load cells has a distance equal to $l/4$ from the model's center of gravity, as shown in Figure 10.

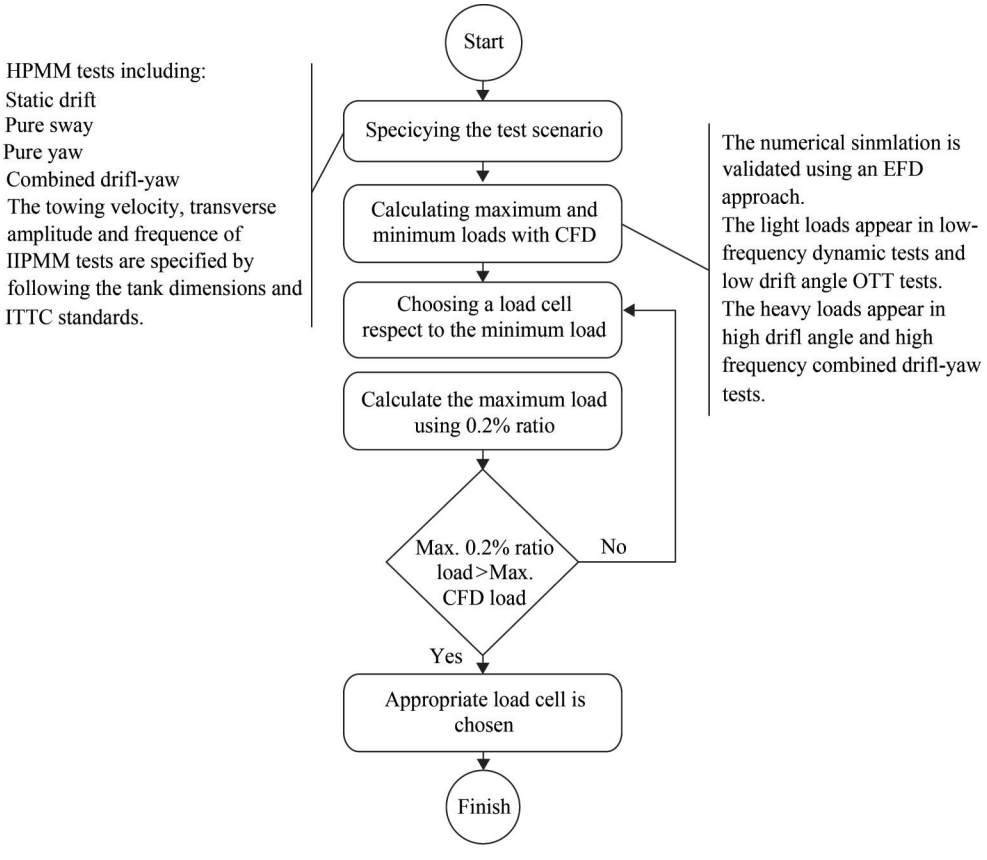

Figure 8 Flowchart of load cell selection

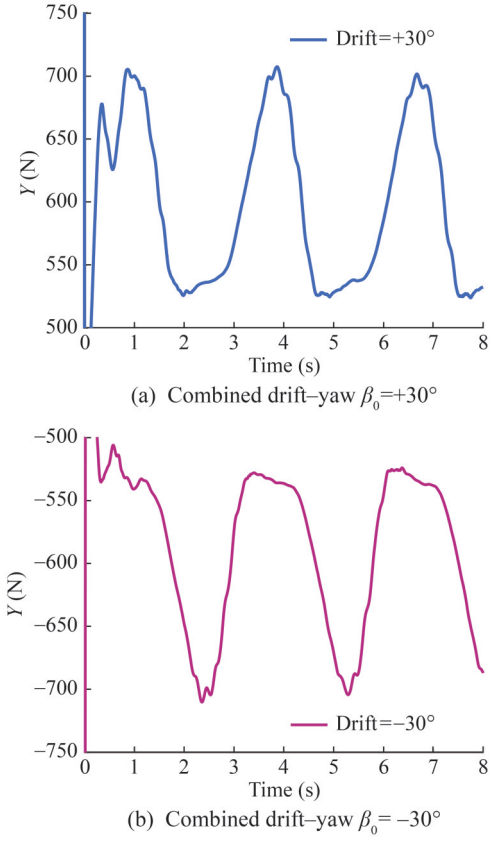

Figure 9 Sway force graphs in terms of time in the combined drift–yaw tests with frequency of 0.35 rad/s

Table 7 Maximum and minimum loads along longitudinal and transversed axes in different test simulations

Test	Axis	Max./Min.	Value (N)
Static drift	*X*	Min.	2.85
		Max.	16.80
	Y	Min.	15.52
		Max.	551.42
Pure sway	*X*	Min.	16.59
		Max.	17.60
	Y	Min.	15.50
		Max.	305.50
Pure yaw	*X*	Min.	15.23
		Max.	17.15
	Y	Min.	0.46
		Max.	19.90
Combined drift–yaw	*X*	Min.	-
		Max.	57.28
	Y	Min.	-
		Max.	709.98

Given the 2.5-meter length of the submarine model and the values of forces and moments applied to the body during the tests, the transverse forces applied to the front and rear load cells can be expressed as follows:

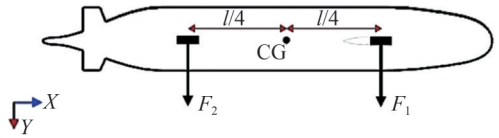

Figure 10 Location of the load cells inside the submarine model

$$F_1 = 0.5\left(Y + \frac{N}{\frac{l}{4}}\right) \tag{22}$$

$$F_2 = 0.5\left(Y - \frac{N}{\frac{l}{4}}\right) \tag{23}$$

where F_1 and F_2 are the transverse forces on the front and rear struts, respectively. The force values acting on each of the load cells related to the heaviest test scenario (combined drift–yaw with $\beta_0 = 30°$ and a frequency of 0.35 rad/s) are depicted in Figure 11. In this test, the maximum force applied to the front load cell is 500 N, and the maximum force in the x direction always has a value smaller than 60.

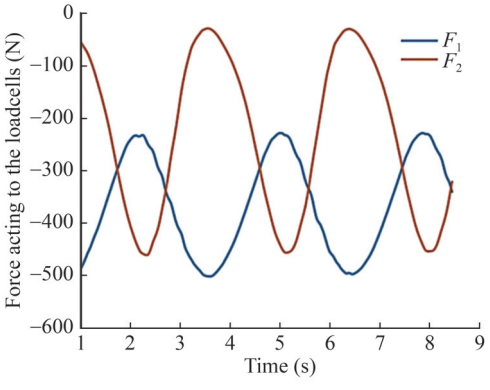

Figure11 Calculated loads acting on each load cell in the heaviest test scenario versus time

4.2 Load cell selection

In this study, the capacity of the load cells is first determined based on numerical results and then according to the proposed method for testing the submarine model in the NIMALA. The specifications of the load cell are presented in the next step. The values of the forces acting on the load cells are listed in Table 8.

The use of two struts with an appropriate profile and two load cells is recommended to perform the captive model test with the HPMM system. The arrangement of the struts is shown in Figure 12.

Table 8 Minimum and maximum forces acting on the load cells

Axis direction	Minimum required accuracy (N)	Maximum capacity of load cells based on 0.2% ratio (N)	Maximum capacity of load cells based on CFD (N)
X	2.85	1 425	57.25
Y	15.50	7 750	709.98

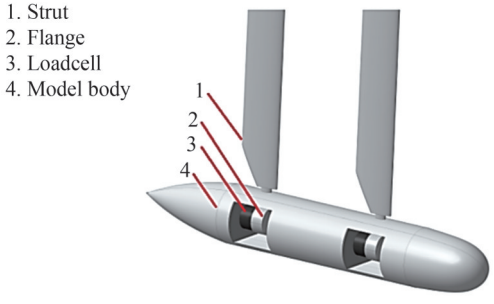

Figure 12 Overview of the conceptual design for submarine testing using the HPMM system

The capacity shown in Table 7 is related to the total force on the model. Given that two 2-component load cells are used in the proposed mechanism, the capacity of each load cell must be measured by considering the effect of the yaw moment. The final capacity of each load cell is specified, as shown in Table 9.

Table 9 Final calculation results for the capacity of the load cells

Number of load cells	Load cell type	F_x (N)	F_y (N)
2	2-components	40	500

5 Conclusions

In this study, the forces acting on the submarine model in HPMM tests were investigated using CFD. The investigations were presented as an instruction flow chart to be used in other similar works. The general results were as follows:

1) Specifying the numerical analysis scenario is essential to determine the appropriate capacity of the load cells. In this scenario, dynamic and static tests must be included, and damping and added mass forces must be determined from the analysis of their results.

2) The maximum load is applied to the body in the combined drift–yaw test, and the minimum load appears in the low-frequency pure yaw test.

3) In determining the input parameters of the considered analyses, the heaviest scenarios should be considered to obtain the maximum forces for calculating the maximum capacity of the load cells. Given that minimum forces are important in calculating the maneuvering hydrodynamic coefficients, the minimum values of the input parameters must also be included.

This research found that numerical approaches can provide an acceptable estimation of the loads acting on HPMM equipment in marine laboratories. In addition to predicting the loads acting on the load cells, an accurate structural and hydrodynamic analysis must be performed on the struts towing the submarine model. This aspect can be a practical subject for further investigations and design of HPMM facilities.

Competing interest The authors have no competing interests to declare that are relevant to the content of this article.

References

Ardeshiri S, Mousavizadegan SH, Kheradmand S (2020) Effect of motion domain and velocity on calculation of underwater vehicle coefficients. Modares Mechanical Engineering 20(1): 117-128

Celik IB, Ghia U, Roache PJ, Freitas CJ, Coleman H, Raad PE (2008) Procedure for estimation and reporting of uncertainty due to discretization in CFD applications. J. Fluids Eng. 130(7): 078001-078004. DOI: 10.1115/1.2960953

Cho YJ, Seok W, Cheon KH, Rhee SH (2020) Maneuvering simulation of an X-plane submarine using computational fluid dynamics. Int. J. Nav. Archit. Ocean Eng. 12: 843-855. DOI: 10.1016/j.ijnaoe.2020.10.001

Feldman J (1979) Revised standard submarine equations of motion. US Navy, Virginia, United States

Ferziger JH, Peric M (2002) Computational methods for fluid dynamics. 3rd edn, Springer, Berlin

Foroushani JA, Sabzpooshani M (2021) Determination of hydrodynamic derivatives of an ocean vehicle using CFD analyses of synthetic standard dynamic tests. Appl. Ocean Res. 108: 102539. DOI: 10.1016/j.apor.2021.102539

Fossen TI (1994) Guidance and control of ocean vehicles. John Wiley & Sons, Chichester, England

Gertler M, Hagen GR (1967) Standard equations of motion for submarine simulation. Naval Ship Research and Development Center. DOI:10.21236/ad0653861

Groves NC, Huang TT, Chang MS (1989) Geometric characteristics of DARPA SUBOFF models (DTRC model Nos. 5470 and 5471). Defense Advanced Research Projects Agency, Virginia, United States, Report DTRC/SHD-1298-01

Holmes EP, Papoulias FA (1995) Prediction of hydrodynamic coefficients utilizing geometric considerations. Master thesis, Naval Postgraduate School, Monterey United States

Huang H, Zhou Z, Li H, Zhou H, Xu Y (2020) The effects of the circulating water tunnel wall and support struts on hydrodynamic coefficients estimation for autonomous underwater vehicles. Int. J. Nav. Archit. Ocean Eng. 12: 1-10. DOI: 10.1016/j.ijnaoe.2019.04.008

Humphreys DE, Watkinson KW (1978) Prediction of the acceleration hydrodynamic coefficients for underwater vehicles from geometric parameters. Naval Coastal System Center, Panama City, United States, Technical Report NCSL-TR-327-78

ITTC (2014) Practical guidelines for ship self-propulsion CFD. ITTC–Recommended Procedures and Guidelines 7.5-03-03-01, 9

ITTC (2017) Uncertainty analysis in CFD verification and validation methodology and procedures. ITTC–Recommended Procedures

and Guidelines 7.5-03-01-01, 1-13
ITTC (2021) Captive model test for underwater vehicles. ITTC – Recommended Procedures and Guidelines 7.5-02-06-07, 9
Kepler JR (2018) Dynamics of a small autonomous underwater vehicle that tows a large payload. Master thesis, Virginia Tech, Blacksburg
Kim D (2023) Experimental study of the hydrodynamic maneuvering coefficients for a BB2 generic submarine using the planar motion mechanism. Ocean Eng. 271: 113428
Pan YC, Zhang HX, Zhou QD (2012) Numerical prediction of submarine hydrodynamic coefficients using CFD simulation. J. Hydrodyn. 24(6): 840-847. DOI: 10.1016/S1001-6058(11)60311-9
Park JY, Kim N, Shin YK (2017) Experimental study on hydrodynamic coefficients for high-incidence-angle maneuver of a submarine. Int. J. Nav. Archit. Ocean Eng. 9(1): 100-113
Roddy RF (1990) Investigation of the stability and control characteristics of several configurations of the DARPA SUBOFF model (DTRC Model 5470) from captive-model experiments. David Taylor Research Center, Bethesda Maryland 20084-5000, DTIC
Shih TH, Liou WW, Shabbir A, Yang Z, Zhu J (1994) A new k-epsilon eddy viscosity model for high Reynolds number turbulent flows model development and validation. Computers & Fluids 24: 227-238. DOI:10.1016/0045-7930(94)00032-T
Siemens (2021) Simcenter STAR-CCM+ user guide. Siemens Digital Industries Software
Vantorre M (2000) Captive manoeuvring tests with ship models: a review of actual practice, based on the 22nd ITTC Manoeuvring Committee Questionnaire. International Conference on Marine Simulation and Ship Manoeuvrability (MARSIM2000), Orlando, 421-438
Yoon H, Longo J, Toda Y, Stern F (2015a) Benchmark CFD validation data for surface combatant 5415 in PMM maneuvers-Part II: Phase-averaged stereoscopic PIV flow field measurements. Ocean Eng. 109: 735-750. DOI: 10.1016/j.oceaneng.2015.09.046
Yoon H, Simonsen CD, Benedetti L, Longo J, Toda Y, Stern F (2015b) Benchmark CFD validation data for surface combatant 5415 in PMM maneuvers-Part I: Force/moment/motion measurements. Ocean Eng. 109: 705-734. DOI: 10.1016/j.oceaneng.2015.04.087
Zhu Z, Kim BS, Wang S, Kim Y (2022) Study on numerical PMM test and its application to KCS hull. Appl. Ocean Res. 127: 103327. DOI: 10.1016/j.apor.2022.103327
Ziabari SY, Mousavizadegan SH (2024) Dynamic oblique towing test (DOTT) to calculate the ship's hull maneuvering derivatives. Ocean Eng. 292: 116526